Dissipation anomaly in a turbulent quantum fluid

Luca Galantucci,[1,2] Em Rickinson,[2] Andrew W. Baggaley,[2] Nick G. Parker,[2] and Carlo F. Barenghi[2,2]

[1] *Istituto per le Applicazioni del Calcolo 'M. Picone', IAC-CNR, Via dei Taurini 19, 00185 Roma, Italy*

[2] *Joint Quantum Centre (JQC) Durham–Newcastle, School of Mathematics, Statistics and Physics, Newcastle University, Newcastle upon Tyne, NE1 7RU, United Kingdom**

(Dated: today)

When the intensity of turbulence is increased (by increasing the Reynolds number, *e.g.* by reducing the viscosity of the fluid), the rate of the dissipation of kinetic energy decreases but does not tend asymptotically to zero: it levels off to a non-zero constant as smaller and smaller vortical flow structures are generated. This fundamental property, called the *dissipation anomaly*, is sometimes referred to as the zeroth law of turbulence. The question of what happens in the limit of vanishing viscosity (purely hypothetical in classical fluids) acquires a particular physical significance in the context of liquid helium, a quantum fluid which becomes effectively inviscid at low temperatures achievable in the laboratory. By performing numerical simulations and identifying the superfluid Reynolds number, here we show evidence for a superfluid analog to the classical dissipation anomaly. Our numerics indeed show that as the superfluid Reynolds number increases, smaller and smaller structures are generated on the quantized vortex lines on which the superfluid vorticity is confined, balancing the effect of weaker and weaker dissipation.

arXiv:2206.14030v2 [physics.flu-dyn] 7 Mar 2023

* l.galantucci@iac.cnr.it

I. INTRODUCTION

It is well known from experiments and numerical simulations of incompressible, homogeneous and isotropic turbulence that, if the fluid's kinematic viscosity ν tends to zero (or, equivalently, if the Reynolds number tends to infinity), the average dissipation rate of turbulent kinetic energy does not decrease to zero, but tends to a finite constant [1, 2]. In other words, the limit of the incompressible Navier-Stokes equation for vanishing viscosity is not the Euler equation, as one would naively expect. This *dissipation anomaly*, led Onsager [3, 4] to conjecture that the solution of the Euler equation is not a smooth velocity field: smaller viscosities are compensated by the creation of motions at smaller and smaller length scales containing much vorticity but little energy. The dissipation anomaly is thus related to the properties of turbulence at the smallest length scales of the flow.

Progress in low temperature physics adds a twist to this story. Turbulence with vanishing viscosity, in fact, is not a mathematical idealisation but can be created in the laboratory by cooling liquid helium (either isotope ^{4}He or ^{3}He) below the critical temperature for Bose-Einstein condensation. Below this temperature, liquid helium becomes a quantum fluid consisting of two interpenetrating components: the inviscid *superfluid* (associated to the quantum ground state) and a gas of thermal excitations (the *normal fluid*) which carries entropy and viscosity. Upon further cooling, the amount of thermal excitations decreases rapidly; for example, ^{4}He becomes effectively a pure superfluid below 1 K. Turbulence is easily generated in this superfluid component by mechanical or thermal stirring, and consists of a disordered tangle of vortex lines of quantised circulation.

Experiments and theory have revealed that, despite the two-fluid nature and the quantised circulation, in certain regimes and at length scales larger than the average inter-vortex spacing ℓ, superfluid turbulence may show properties similar to ordinary (classical) turbulence [5, 6]. A notable example is the observation in liquid helium [7, 8] of the famed Kolmogorov energy spectrum [9] revealing an energy cascade at those large length scales. The aim of this letter is to present evidence of an additional similarity between classical and quantum turbulence, this time occurring at the smallest length scales of the flow: a superfluid analog of the classical dissipation anomaly. After defining the superfluid Reynolds number, we shall briefly introduce our numerical model and then present and discuss our finding.

We stress that the aim of our study is to draw a parallel between the dissipation anomaly in classical fluids which arises from viscous effects and the dissipation anomaly in quantum turbulence which, as we shall see, arises at decreasing temperature from the mutual friction [10] between the vortex lines and the normal fluid. Hence, in our numerical simulations of quantum turbulence, the temperature must be high enough that the energy is indeed dissipated by mutual friction at lengthscales larger than the vortex core radius, a_0, and not by phonon emission (in ^{4}He) or excitation of Carol-Matricon states (in ^{3}He). These two effects would occur if the energy cascade continued until the smallest scales of the flow ($\approx a_0$). This is why our model is not the Gross-Pitaevskii equation which has been found to describe the dissipation of incompressible kinetic energy into phonons at zero temperature [11].

II. MODEL

A. Superfluid Reynolds Number

The first step is to identify the superfluid Reynolds number (a measure of the intensity of the turbulence) by making careful analogy with classical fluid dynamics. Classical fluids obey the Navier-Stokes equation. If ν is the kinematic viscosity of the fluid, and U and L are characteristic speed and length scales of the flow respectively, the dimensionless Navier-Stokes equation, written in terms of the vorticity $\boldsymbol{\omega} = \nabla \times \mathbf{v}$, where $\mathbf{v}$ is velocity, has the form

$$\frac{\partial \boldsymbol{\omega}}{\partial t} = \nabla \times (\mathbf{v} \times \boldsymbol{\omega}) + \frac{1}{Re}\nabla^2 \boldsymbol{\omega}, \tag{1}$$

where $Re = UL/\nu$ is the Reynolds number. The two terms at the right hand side of Eq. (1) describe respectively inertia and viscous dissipation. Turbulence arises when $Re \gg 1$, *i.e.* when inertia is much larger than dissipation. In superfluid helium, vorticity is not a continuous field but is concentrated in thin vortex lines of fixed atomic thickness, a_0, and fixed circulation, $\kappa = h/m$, where h is Planck's constant and m the mass of the relevant boson (an atom for bosonic ^{4}He, a Cooper pair for fermionic ^{3}He). The Hall-Vinen-Bekharevich-Khalatnikov (HVBK) equations [12] provide a convenient coarse-grained, continuum model of finite temperature superfluid hydrodynamics of fluid parcels threaded by a large number of vortex lines. When the HVBK equations are applied to fully developed turbulence, vortex-tension effects are negligible (being proportional to $1/Re_\kappa = \kappa/(UL) \ll 1$) and the governing dimensionless equation for the superfluid vorticity $\boldsymbol{\omega}_s$ is

$$\frac{\partial \boldsymbol{\omega}_s}{\partial t} = (1-\alpha')\nabla \times (\mathbf{v}_s \times \boldsymbol{\omega}_s) + \alpha \nabla \times [\hat{\boldsymbol{\omega}}_s \times (\boldsymbol{\omega}_s \times \mathbf{v}_s)], \tag{2}$$

where α and α' are known temperature-dependent friction coefficients arising from the interaction of vortex lines with the normal fluid (which, for the sake of simplicity, we assume to be at rest). Following Finne *et al.* [13] and the classical definition of Reynolds number, we identify the superfluid Reynolds number Re_s as the ratio of inertial forces (the first term at the right hand side of Eq. (2)) to dissipative forces (the second term), obtaining

$$Re_s = \frac{(1-\alpha')}{\alpha}. \tag{3}$$

Note that Re_s does not depend on extrinsic parameters (U and L) but only on temperature-dependent fluid properties (α and α'), unlike the classical Reynolds number. We stress that experiments and numerical simulations [13] confirm that the transition to turbulence can indeed be predicted using Eq. (3).

B. Numerical Model

The second step consists of numerical simulations of superfluid turbulence in which we compute the dissipation rate of turbulent kinetic energy, ϵ, as a function of Re_s. We employ the well-established vortex filament method (VFM) [14, 15] which models superfluid hydrodynamics at length scales smaller than the average inter-vortex distance, ℓ, but much larger than the vortex core radius, a_0. Unlike the HVBK framework, the VFM still describes the discrete nature of superfluid vorticity. Vortex lines are described as one-dimensional filaments, $\mathbf{s}(\xi, t)$, ξ being the arc length and t time, which move according to the balance of Magnus and friction forces. The velocity of a vortex line at point $\mathbf{s}(\xi, t)$ is

$$\frac{\partial \mathbf{s}}{\partial t} = \mathbf{v}_s - \alpha \mathbf{s}' \times \mathbf{v}_s + \alpha' \mathbf{s}' \times (\mathbf{s}' \times \mathbf{v}_s), \tag{4}$$

where

$$\mathbf{v}_s(\mathbf{s}(\xi,t),t) = \frac{\kappa}{4\pi} \oint_{\mathcal{T}} \frac{\mathbf{s}'(\xi_1,t) \times (\mathbf{s}(\xi,t) - \mathbf{s}(\xi_1,t))}{|\mathbf{s}(\xi,t) - \mathbf{s}(\xi_1,t)|^3} d\xi_1, \tag{5}$$

the line integral (desingularized as in [16]) extending over the entire vortex configuration $\mathcal{T}$, and $\mathbf{s}' = \partial \mathbf{s}/\partial \xi$ being the unit tangent at $\mathbf{s}$. The local curvature (the inverse of the local radius of curvature) is defined as $\zeta = |\mathbf{s}''|$, where $\mathbf{s}'' = \partial^2 \mathbf{s}/\partial \xi^2$. In the VFM, each filament is discretized into a variable number of oriented line elements held at a distance $\Delta\xi \in [\delta/2, \delta]$; here we choose $\delta = 0.02\,\mathrm{cm}$, and check results by halving δ. Each simulation is performed at temperature T in a periodic cube of size $D = 1$ cm. The time integration is a Runge-Kutta 4th order scheme, $\Delta t = 5 \times 10^{-3}$ s being the typical time step. Reference [15] gives more details, including vortex reconnections performed algorithmically when two filaments collide.

A fully realistic model of turbulent ^{4}He would need to couple Eq. (4) to a Navier-Stokes equation for the turbulent normal fluid velocity $\mathbf{v}_n$, suitably modified to include the friction arising from the relative motion of vortex lines and $\mathbf{v}_n$. Due to computational costs, such coupled dynamics of vortex lines and normal fluid has been attempted only for particular vortex configurations [17–19] or turbulent transients [20, 21]: fully developed, statistically-steady two-fluid turbulence has not been achieved yet. Therefore, we limit this investigation to the following idealised but computationally simpler form of superfluid turbulence: a tangle of vortex lines whose dissipative motion with respect to a quiescent normal fluid is modelled by Eq. (4) at the mesoscale level. This simpler form still allows us to make progress into a problem never addressed before. It is worth stressing that although idealised for ^{4}He, our model is realistic for ^{3}He-B, whose normal component is so viscous that it is usually assumed to be at rest with respect to the container (see Appendix A).

III. RESULTS

To establish a turbulent flow, we start with a vortex ring of radius $R = D/2$ at the centre of the box, and inject randomly oriented vortex rings of the same radius R at random positions and at a prescribed rate $\dot{L}_{inj}$ (a

similar procedure was used in the experiment of Walmsley and Golov [22], although their injection was not isotropic). The injected vortex rings interact with other vortex lines, reconnect, and a turbulent vortex tangle is formed, see Fig. 1 (a,b).

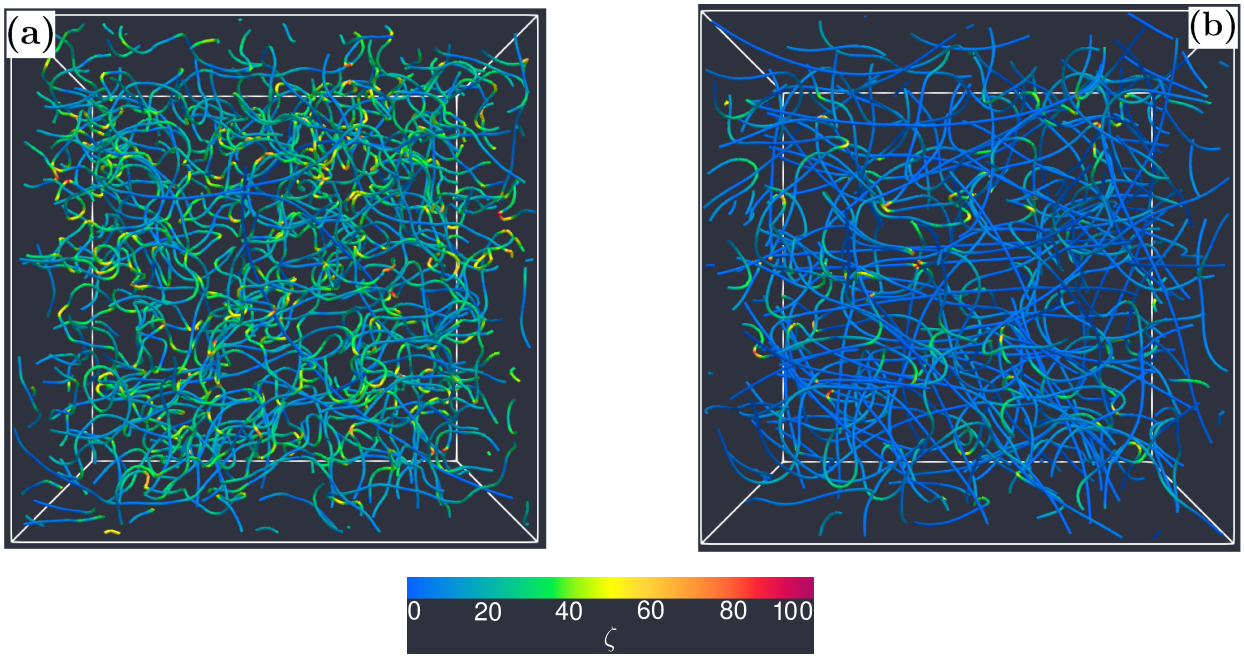


FIG. 1. Snapshot of vortex tangles in the saturated steady-state regime at $\overline{L} \sim 120\text{cm}^{-2}$, for: (a) $Re_s = 29$ and $\dot{L}_{inj} = 3.35\text{cm}^{-2}\text{s}^{-1}$(corresponding to pink open diamond symbols in Fig. 2 (a)); (b) $Re_s = 1.25$ and $\dot{L}_{inj} = 22.50\text{cm}^{-2}\text{s}^{-1}$(corresponding to violet filled diamond symbols in Fig. 2 (a)). Vortex lines are colour-coded according to the local curvature ζ (in cm^{-1}, legend at the bottom); note the larger values of ζ at the larger Re_s.

Without continual injection, the tangle would decay due to the friction suffered by the vortex lines as they move in the quiescent normal fluid background. The statistically-steady state of turbulence which is achieved after an initial transient T_{eq} is independent of the initial condition (injection and dissipation balancing each other). In this state, the vortex line density L (defined as the vortex line length per unit volume) fluctuates around a constant saturation value $\overline{L}$, as illustrated in Fig. 2 (b). The diameter of the injected rings is equal to the box size and hence energy is mainly supplied to the turbulence at scales larger than ℓ [23, 24] (see also Appendix B). As $\mathbf{v}_n$ is kept static, mutual friction dissipates energy at all lengthscales, implying that the turbulence thus generated is not quasi-classical (where by the latter we intend a quantum turbulent flow where at large scales the two fluid components are coupled by mutual friction and hence undergo a coupled energy cascade with little dissipation until a lengthscale $\sim \ell$ is reached [5, 25, 26]). However, at scales larger than ℓ, we still do observe the emergence of an inertial-range energy cascade and the subsequent Kolmogorov energy spectrum $\hat{E}(k) \sim k^{-5/3}$ (see Fig. 4 (a) and Appendix B), as the largest eddy turnover time $\tau_D = (D^2/\epsilon)^{1/3}$ is never significantly larger than the mutual friction dissipative time-scale $\tau_{mf} = 1/(\alpha\kappa\overline{L})$. Our computational box is not large enough that $\tau_D \gg \tau_{mf}$, which would make friction dominant at large scales creating a crossover to a k^{-3} scaling [26–29].

When in our simulations the mentioned Kolmogorov energy cascade reaches scales $\sim \ell$, the energy transfer towards smaller scales $k \gtrsim k_\ell = 2\pi/\ell$ creates Kelvin waves (KWs) of shorter and shorter wavelengths on individual vortex lines. In our temperature range ($T \geq 1.3$K), this KW cascade [30–32] is limited by the friction with the normal fluid [25, 27, 33].

In order to assess the effect of turbulent intensity on the rate of dissipation of kinetic energy, ϵ, we choose 11 temperature values in the range $1.3\text{ K} \leq T \leq 2.16\text{ K}$, and 8 injection rates $\dot{L}_{inj} = (dL/dt)_{inj}$ in the range $0.34\text{ cm}^{-2}\text{s}^{-1} \leq \dot{\text{L}}_{\text{inj}} \leq 22.50\text{ cm}^{-2}\text{s}^{-1}$. The saturation value, $\overline{L}$, increases with $\dot{L}_{inj}$ and decreases with T. At saturation, on average $\dot{L}_{tot} = \dot{L}_{inj} + \dot{L}_{decay} = 0$, leading to $\overline{L} = \sqrt{2\pi\dot{L}_{inj}/(\kappa\chi_2)}$ [34], as confirmed by our numerical simulations, see Fig. 2 (a). The values of χ_2 extrapolated from our data are consistent with recent studies [35].

To extract values of the energy dissipation rate ϵ as a function of Re_s we select the numerical simulations corresponding to a constant value of $\dot{L}_{inj}$ (we choose $\dot{L}_{inj} = 3.35\text{ cm}^{-2}\text{s}^{-1}$), implying that the only varying physical parameter among the distinct simulations is T (or, equivalently, Re_s). The selected simulations are enclosed in the red

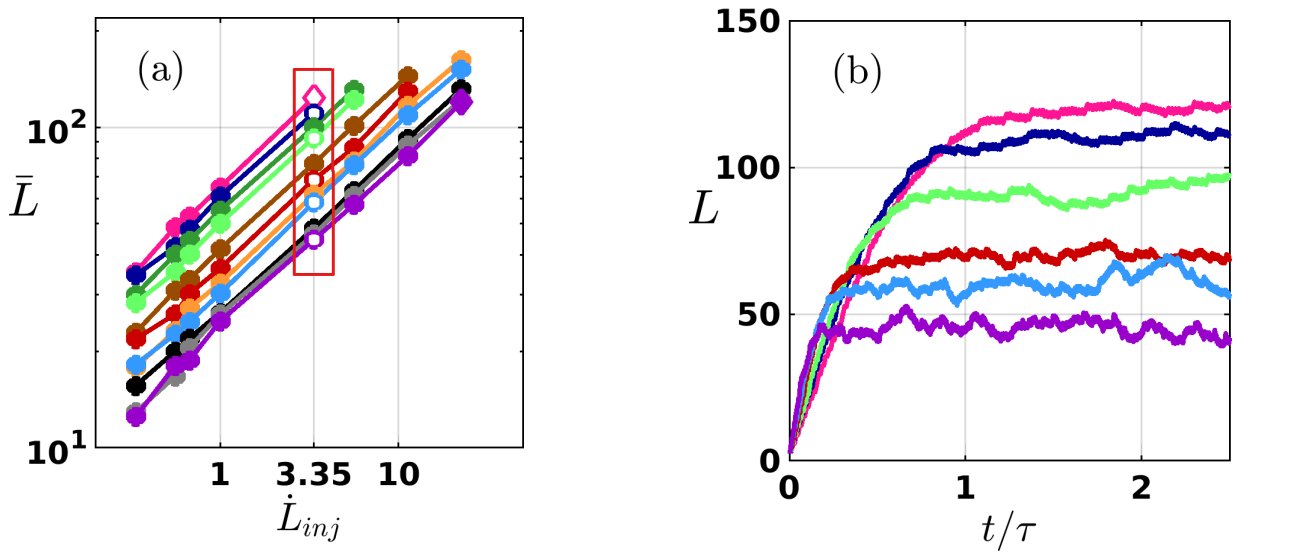


FIG. 2. (a): Vortex line density at saturation, $\overline{L}$ (in cm^{-2}), *vs* injection rate $\dot{L}_{inj}$ (in cm^{-2}s^{-1}) for Re_s =1.25 (violet), 1.34 (grey), 1.50 (black), 2.06 (cyan), 2.51 (yellow), 3.30 (red), 4.96 (brown), 9.84 (light green), 13.09 (dark green), 19.66 (blue), 29.00 (pink). (b): Time evolution of the vortex line density L (in cm^{-2}) *vs* time t/τ, at $\dot{L}_{inj} = 3.35$ cm^{-2}s^{-1}, for different values of Re_s (colors as in (a)), corresponding to simulations indicated with open symbols in (a).

rectangle in Fig. 2 (a)) and the temporal evolution of the vortex line density L for this set of simulations at constant $\dot{L}_{inj}$ is illustrated in Fig. 2 (b). For each Re_s, after the transient T_{eq}, we calculate the dissipation rate ϵ every time interval $\tau = 2\pi/(\kappa\overline{L})$ via the following integral,

$$\epsilon(t_i) = \frac{1}{\rho_s D^3} \oint_{\mathcal{T}(t_i)} \mathbf{f}_{ns}(\xi, t_i) \cdot \dot{\mathbf{s}}(\xi, t_i) \mathrm{d}\xi \ , \tag{6}$$

where $-\mathbf{f}_{ns} = -\gamma_0 \, \dot{\mathbf{s}} - \gamma_0' \, \mathbf{s}' \times \dot{\mathbf{s}}$ is the mutual friction force per unit length which the normal fluid exerts on a superfluid vortex line element [36] (γ_0 and γ_0' being a reformulation of mutual friction coefficients α and α'), and $\mathcal{T}(t_i)$ is the configuration of vortex tangle at time $t_i = T_{eq} + i \cdot \tau$ (with $i = 1, \ldots, 10$).

At the same times t_i, we evaluate the root-mean-square velocity fluctuation $U(t_i)$, where $3U^2(t_i)/2 = E(t_i)$ is the turbulent kinetic energy per unit mass, and the turbulent integral scale $I(t_i) = \dfrac{\pi}{2U^2} \displaystyle\int_0^\infty \frac{\hat{E}(k, t_i)}{k} \, \mathrm{d}k$, where $\hat{E}(k, t_i)$ is the one-dimensional energy spectra so that $E(t_i) = \int_0^\infty \hat{E}(k, t_i) \, \mathrm{d}k$. Finally, we average over time ϵ, U and I and compute the normalised energy dissipation rate as $\widetilde{\epsilon} = \langle \epsilon \rangle \langle I \rangle / \langle U \rangle^3$ ($\langle \cdot \rangle$ indicating time-averaged quantities), in order to mimic the normalisation performed in classical turbulence. This procedure is repeated for each Re_s and the curve $\widetilde{\epsilon}(Re_s)$ is plotted in Fig. 3 (a), red curve.

Fig. 3 (a) shows our main result: the normalised energy dissipation rate $\widetilde{\epsilon}$ decreases and then flattens out as the superfluid Reynolds number, Re_s, is increased: the similarity with the classical dissipation anomaly [1, 2] is striking.

A. Interpretation of the results

We examine the geometry of the vortex tangle. Fig. 3 (b) shows the probability density function (PDF) of the curvature ζ along the vortex lines as a function of Re_s. Clearly, increasing Re_s shifts this distribution towards higher ζ, hence towards smaller length scales $1/\zeta$. The small-scale (large ζ) vortex structures generated at lower temperatures survive because of the reduced friction dissipation and, as a consequence, the probability of observing structures at scales smaller than ℓ increases as Re_s increases (see Appendix C). The energy cascade towards small scales can be described as a shift of PDF(ζ) towards high curvatures, starting from the injected value $\zeta_0 = 1/R$ (see Appendix D).

As in classical turbulence, smaller friction (decreasing values of α) leads to the excitation of smaller scale motions. The flattening of the $\widetilde{\epsilon}$ curve can be understood using the following simple argument which is only strictly valid for Vinen turbulence, but is likely to be applicable, at least qualitatively, to other quantum turbulent regimes, as the dissipation stems from the small-scale dynamics (see Fig.4 (b) and subsequent discussion), independently of the large

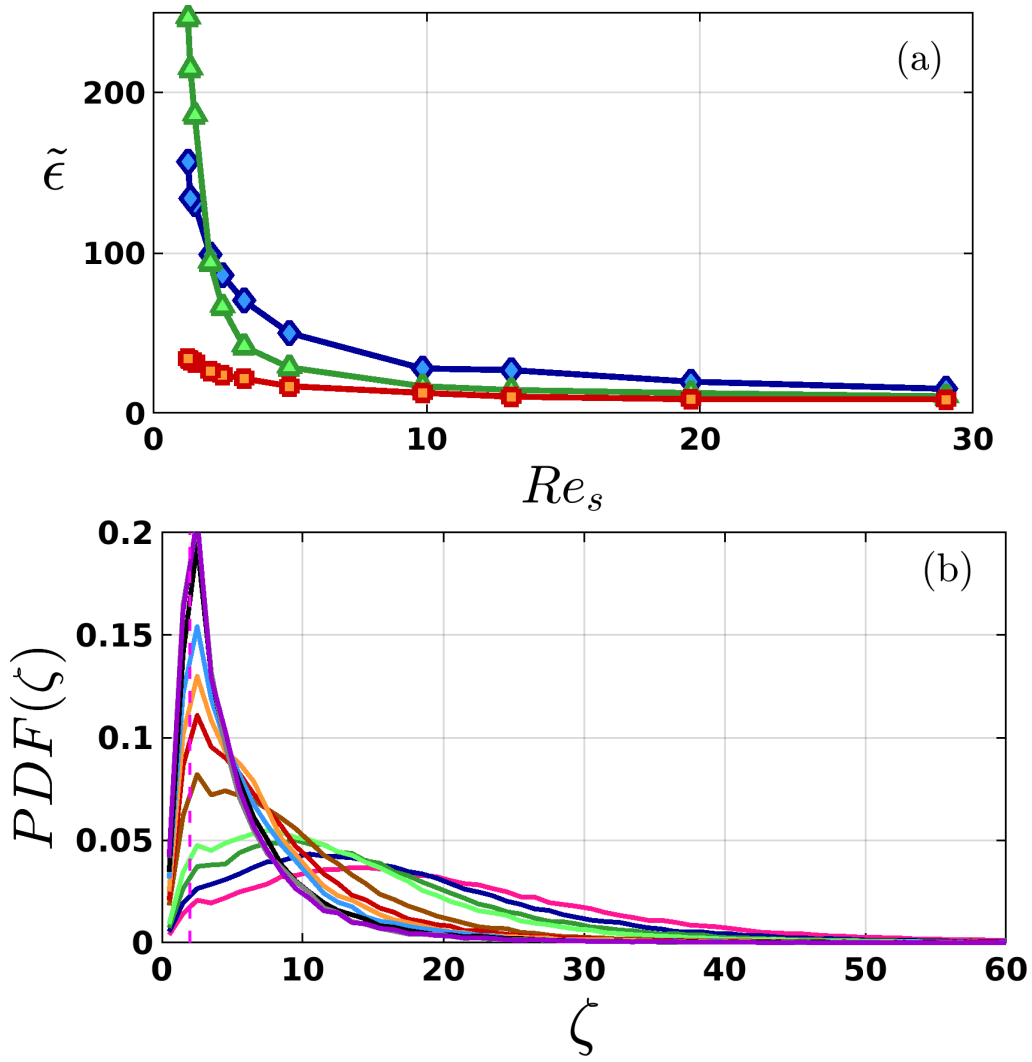


FIG. 3. (a): Normalised energy dissipation rate, $\widetilde{\epsilon}$, *vs* superfluid Reynolds number, Re_s, at $\dot{L}_{inj} = 3.35\text{cm}^{-2}\text{s}^{-1}$. Red curve: injected vortex ring radius $R = D/2$; Green curve: $R = D/8$; Blue curve: $R \gtrsim \bar{\ell}/2$. (b): probability density function of the curvature PDF(ζ) (in cm) *vs* curvature ζ (in cm^{-1}) at increasing Re_s, for $\dot{L}_{inj} = 3.35\text{cm}^{-2}\text{s}^{-1}$ and $R = D/2$. Colors as in Fig. 2. The vertical dashed magenta line marks the curvature of the injected rings $\zeta_0 = 2/D$.

scale flow features. The kinetic energy per unit mass $f(t)$ of a vortex ring of radius R at time t is $f(t) \sim \kappa^2 R(t)/\bar{\ell}^3$ (where $\bar{\ell}$ is the average inter-vortex spacing at saturation). The dissipation rate ϵ is hence given by

$$\epsilon = -df/dt = -\kappa^2 \dot{R}/\bar{\ell}^3 = \alpha\kappa^3\zeta/\bar{\ell}^3 \simeq \alpha\kappa^3\zeta^4 \ , \tag{7}$$

where we have employed the well-known shrinking rate of a vortex ring in a quiescent normal fluid, $\dot{R} \sim -\alpha\kappa/R$ (cf. Eq. (4)), and the relation $\langle\zeta^2\rangle \propto \bar{\ell}^{-2}$ [14]. As Re_s increases, the decreasing value of α is thus compensated by larger curvatures ζ on the vortex lines, flattening $\widetilde{\epsilon}$ as shown in Fig. 3 (a) (red curve). The presence of larger values of ζ (smaller structures) along the vortex lines as Re_s increases is clearly visible in Fig. 1 (a,b). This behaviour is analogous to the scenario observed in classical turbulence where the dissipation rate $\epsilon_{class} = (\nu/2)(\partial v_i/\partial x_j + \partial v_j/\partial x_i)^2$ tends to a finite constant as decreasing viscosity is balanced by increasing velocity gradients. Our results hence show that the curvature of vortices in quantum turbulence play the same role of enstrophy in classical turbulence, as, in terms of dissipative effects, small-scale one-dimensional structures on superfluid vortices correspond to the classical dissipative eddies.

To evaluate the importance of the smallest scales ($k > k_\ell$) in dissipating the superfluid kinetic energy, we calculate the fraction $\epsilon_{<\ell}$ of total dissipation arising from the motion of vortexline elements with curvature $\zeta > 1/\ell$. The result is illustrated in Fig. 4 (b) (red curve) where we observe that $\epsilon_{<\ell}$ is larger than 0.75 for all Re_s. The value of $\epsilon_{<\ell}$ close

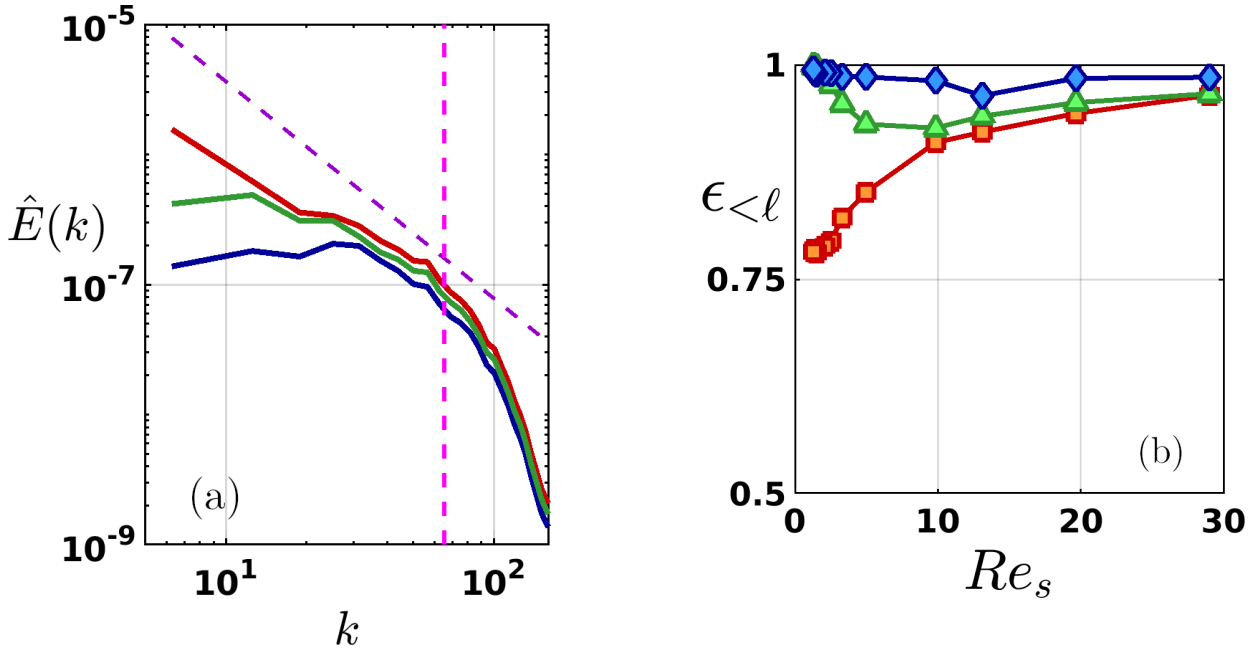


FIG. 4. (a): time averaged superfluid kinetic energy spectra $\hat{E}(k)$ (arbitrary units) as a function of wavenumber k (cm^{-1}) at saturation for $\dot{L}_{inj} = 3.35\mathrm{cm}^{-2}\mathrm{s}^{-1}$ and $Re_s = 29$ ($\hat{E}(k)$ for lower Re_s in Appendix B). Vertical pink and oblique violet dashed lines indicate k_ℓ and the $k^{-5/3}$ scaling, respectively. (b): fraction $\epsilon_{<\ell}$ of total dissipation arising from lengthscales smaller than ℓ. Colors, as in Fig. 3 (a) refer to different radii of the injected vortex rings.

to 1 for the largest Re_s and its slight decrease for decreasing Re_s stems from the fact that $\tau_{mf} \to \tau_D$ as $Re_s \to 0$, consistently with previuos theoretical predictions [27].

This predominant role played by the smallest scales in the dissipation implies that the superfluid analog to the classical dissipation anomaly does not depend on the mechanism transferring the energy to such small scales. To show this independence from the largest scales, we repeat our numerical experiment injecting smaller rings of radii $R = D/8$ and $R \gtrsim \bar{\ell}/2$. These injection protocols produce Vinen-like energy spectra which peak at intermediate scales [37], as shown in Fig. 4 (a, green and blue curves). Despite this non-classical aspect at large scales, the dissipation anomaly is still clearly evident, see Fig. 3 (a, green and blue curves). This result does not depend on the normalisation, as shown in Appendix E.

B. Numerical resolution of the small length scales

As increasing Re_s excites smaller length scales along the vortex lines, it is natural to ask whether our numerical discretization correctly resolves these small scales. To assess our numerical resolution we have repeated all the simulations replacing δ with $\delta/2$ and in the calculation of $\widetilde{\epsilon}$ we have rejected the results of simulations which do not satisfy strict criteria regarding the saturation value $\overline{L}$ and curvature ζ (see Appendix F). In practice, our strict criterion limits us to temperatures above $T \approx 1.3$ K, above the appearance of scaling behaviour for the KW cascade [30–32]. Therefore, our model does not suffer the numerical dissipation at the small length scales which occurs in the VFM if the temperature is set to zero [38].

IV. CONCLUSIONS

Our numerical investigation shows that to understand the small-scale dynamics of superfluid turbulence one has to consider the full distribution of the curvature along the vortex lines, not simply the average value. We have shown that, superfluid turbulence displays the same dissipation anomaly which is observed in classical turbulence: the effect of increasing Reynolds number is the creation of smaller length scales. This result concerning the smallest length scales of turbulence adds insight into the remarkable analogies between classical turbulence and superfluid turbulence already noticed at the largest length scales [5, 26]. It is a striking result, because it deals with lengthscales smaller

than the average inter-vortex distance, where classical and quantum turbulence have always been believed to differ [29]. The role of the quantisation of circulation is thus to *constrain* these dissipative structures to live on vortex lines rather than in the bulk of the flow.

Our results illustrate the nature and the dynamical origin of the recent observation of a dissipation anomaly obtained by forcing KWs in superfluid ^{3}He-B [39], contributing to the lively debate regarding in which turbulent systems dissipative anomaly manifests itself [40].

ACKNOWLEDGMENTS

Acknowledgments.— We thank Giorgio Krustulovic and Ladislav Skrbek for useful discussions, and acknowledge the support of EPSRC grant EP/R005192/1. LG acknowledges the support of Istituto Nazionale di Alta Matematica (INdAM).

Appendix A: Application to ^{3}He

In the numerical simulations with the VFM we use values of parameters relative to ^{4}He: $\kappa = h/m = 9.97\times10^{-7}$ m^2/s (where h is Planck's constant and m the mass of one atom of ^{4}He), $a_0 \approx 10^{-10}$ m, α and α' from Ref. [41]. However our main conclusions are also relevant to ^{3}He-B for the following reasons.

(i): In ^{3}He the relevant boson is a Cooper pair consisting of two ^{3}He atoms (each having mass equal to 3/4 of m), therefore the quantum of circulation is 2/3 of the value in ^{4}He. This difference implies a small rescaling of the characteristic velocity, hence of time, for example when judging the duration of numerical simulations, such as the simulations reported in Fig. 2 (b).

(ii): The different values of the friction coefficients imply a simple rescaling of T, hence of Re_s in Figs. 3 (a) and 4 (b).

(iii): The mesoscopic length scales described by the VFM are much larger than the vortex core radius in both ^{4}He and ^{3}He ($a_0 \approx 10^{-6}$cm);

Appendix B: Energy spectra

In this Appendix B we illustrate the behaviour of the time-averaged energy spectra $\hat{E}(k)$ for different injected ring radii. In Fig. 5 (a) and (b) we report the time-averaged spectra $\hat{E}(k)$ *vs* wavenumber k for injected ring radii $R = D/2$ and $R \gtrsim \bar{\ell}/2$, respectively. The distinct curves reported in Fig. 5 (a) and (b) correspond to all values of Re_s employed in the numerical simulations (the color legend coincides with the legend used in Fig. 2). The injection rate $\dot{L}_{inj} = 3.35\text{cm}^{-2}\text{s}^{-1}$ is fixed.

In Fig. 5 (a) we observe that when the ring is injected at the largest scales of the flow, the energy spectrum $\hat{E}(k)$ is precisely peaked at scale D. In addition, at these large scales we can observe the emergence of a Kolmogorov $k^{-5/3}$ spectrum. As illustrated in the main manuscript, this Kolmogorov spectrum does *not* imply that the quantum turbulence that we generate is quasi-classical (where by the latter we intend a quantum turbulent flow where at large scales the two fluid components are coupled by mutual friction and hence undergo a coupled energy cascade with little dissipation until a lengthscale $\sim \ell$ is reached). As the normal fluid is in fact kept quiescent, the mutual friction force acts at all lengthscales. However, given that the mutual friction characteristic time-scale is never sufficiently small when compared to the eddy turnover time, we still observe an the emergence of an inertial-range Kolmogorov spectrum at all Re_s. [26–29].

On the other hand, in Fig. 5 (b), as the energy is injected at scales comparable to the average inter-vortex spacing at saturation, we observe Vinen-like (often also called ultra-quantum) energy spectra, peaked at intermediate lengthscales, for all values of Re_s.

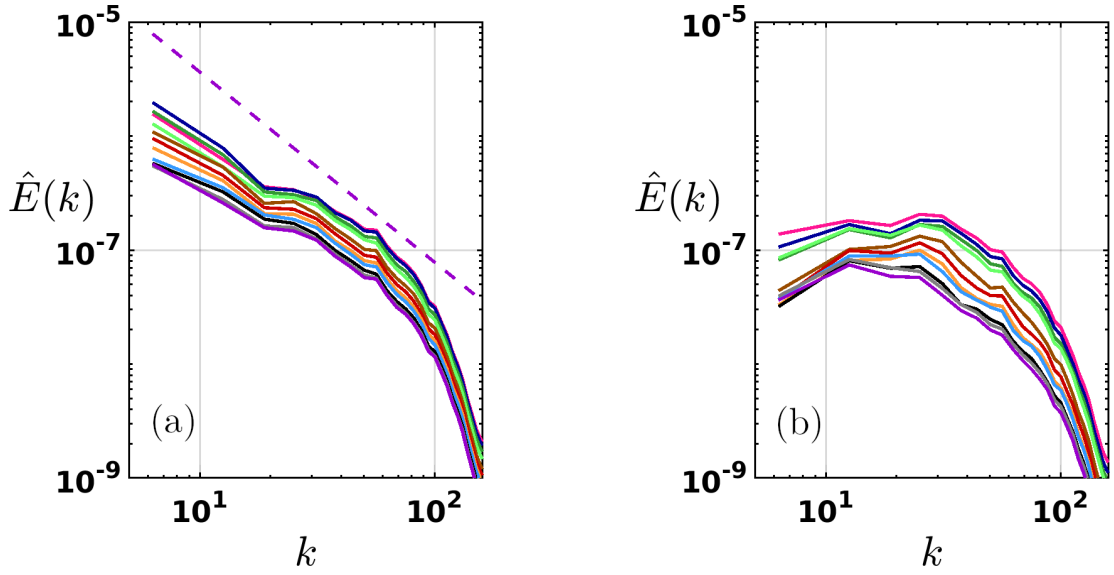


FIG. 5. Superfluid kinetic energy time-averaged spectra $\hat{E}(k)$ (arbitrary units) as a function of wavenumber k (cm^{-1}) for $\dot{L}_{inj} = 3.35\mathrm{cm}^{-2}\mathrm{s}^{-1}$. Different colors refer to distinct values of Re_s: 1.25 (violet), 1.34 (grey), 1.50 (black), 2.06 (cyan), 2.51 (yellow), 3.30 (red), 4.96 (brown), 9.84 (light green), 13.09 (dark green), 19.66 (blue), 29.00 (pink). (a): radius of injected rings $R = D/2$; (b): radius of injected rings $R \gtrsim \bar{\ell}/2$. The dashed violet curve in (a) indicates the Kolmogorov $k^{-5/3}$ energy spectrum.

Appendix C: Probability of observing scales smaller than ℓ

In this section of the Appendix, in Fig. 6 (top) we report the Probability Density Function of the curvature $PDF(\zeta)$ for selected values of $Re_s = 1.25, 2.5, 9.8, 29$, indicating the corresponding value $\zeta_\ell = 1/\ell$, which increases for increasing Re_s. This figure is almost identical to Fig. 3 (a), the only differences being the the indication of ζ_ℓ and the selection of fewer values of Re_s in order to ease the readability of the figure. On the basis of this data, we have calculated the probability $P(\zeta > \zeta_\ell)$ of observing structures at length scales smaller than ℓ as a function of the superfluid Reynolds number Re_s, reporting the results in Fig. 6 (bottom). Fig. 6 shows that structures at scales smaller than ℓ exist and that the probability of observing such small structures increases as Re_s increases.

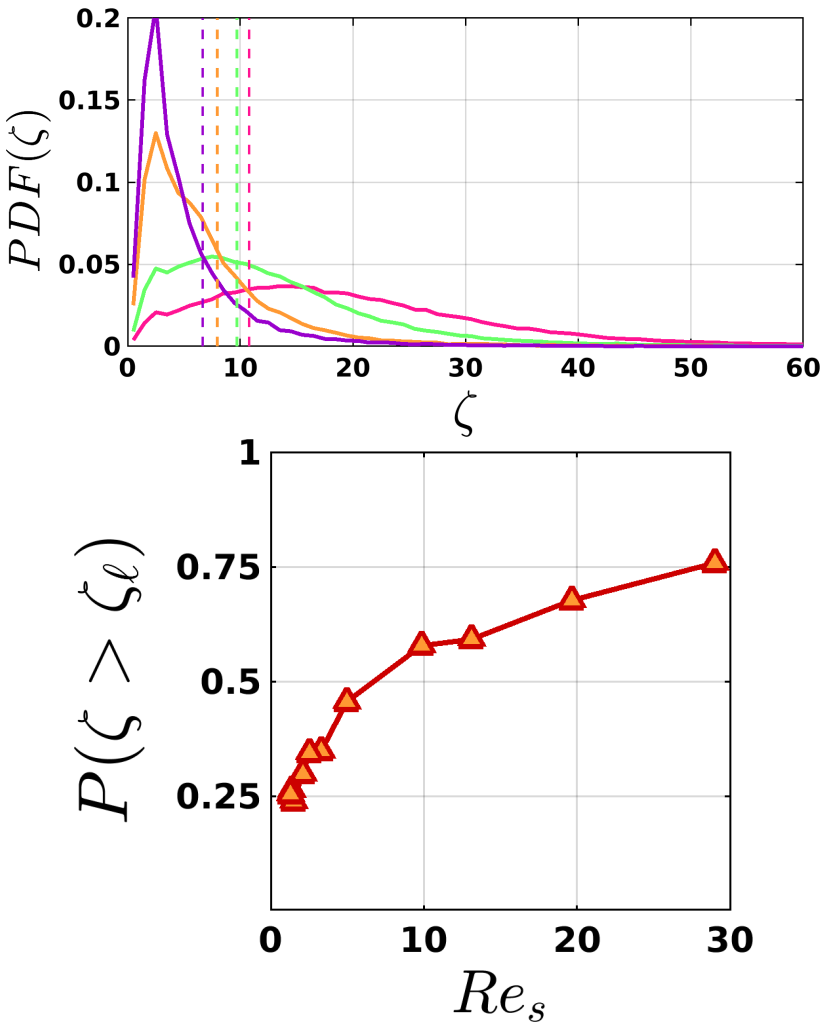


FIG. 6. (Top): $PDF(\zeta)$ for $Re_s = 1.25$, 2.5, 9.8, 29 (violet, orange, light green and magenta solid lines, respectively) for the set of simulations where the radius of the injected rings $R = D/2$. The vertical dashed lines correspond to $\zeta_\ell = 1/\ell$ for each Re_s; (Bottom): Probability $P(\zeta > \zeta_\ell)$ of observing structures at length scales smaller than ℓ as a function of the superfluid Reynolds number Re_s.

Appendix D: Temporal evolution of curvature

In this Appendix D, we show the temporal evolution of the PDF of the curvature ζ. We focus on two simulations, whose vortex-tangle snapshots are illustrated in Fig. 1 (a) and (b). In the first simulation, $Re_s = 29$ and $\dot{L}_{inj} = 3.35\text{cm}^{-2}\text{s}^{-1}$ (corresponding temporal evolution of PDF(ζ) reported in Fig. 7 (top)), in the second $Re_s = 1.25$ and $\dot{L}_{inj} = 22.50\text{cm}^{-2}\text{s}^{-1}$ (PDFs showed in Fig. 7 (bottom)). At saturation, in both numerical simulations the vortex line density is approximately equal to 120cm^{-2}.

In both simulations, the radius of the injected vortex rings is $R = D/2$ and the corresponding curvature $\zeta = 1/R = 2/D$ is indicated in Fig. 7 (top) and (bottom) by a magenta dashed vertical line. The pattern which emerges from Fig. 7 is clear: as the rings are injected, by interacting and reconnecting with the pre-existing tangle, smaller structures with corresponding higher curvatures are generated. As Re_s is increased (or, equivalently, as temperature is decreased), the smaller value of the friction coefficients allows the generation and the survival of smaller structures with higher values of curvature: the resulting PDF(ζ) is more shifted to the right. It is this generation of smaller scale structures as Re_s increases which is responsible for the observed plateau of the normalized kinetic energy dissipation $\widetilde{\epsilon}$ at large Re_s, reported in Fig. 3 (a) and which is the principal finding of our work.

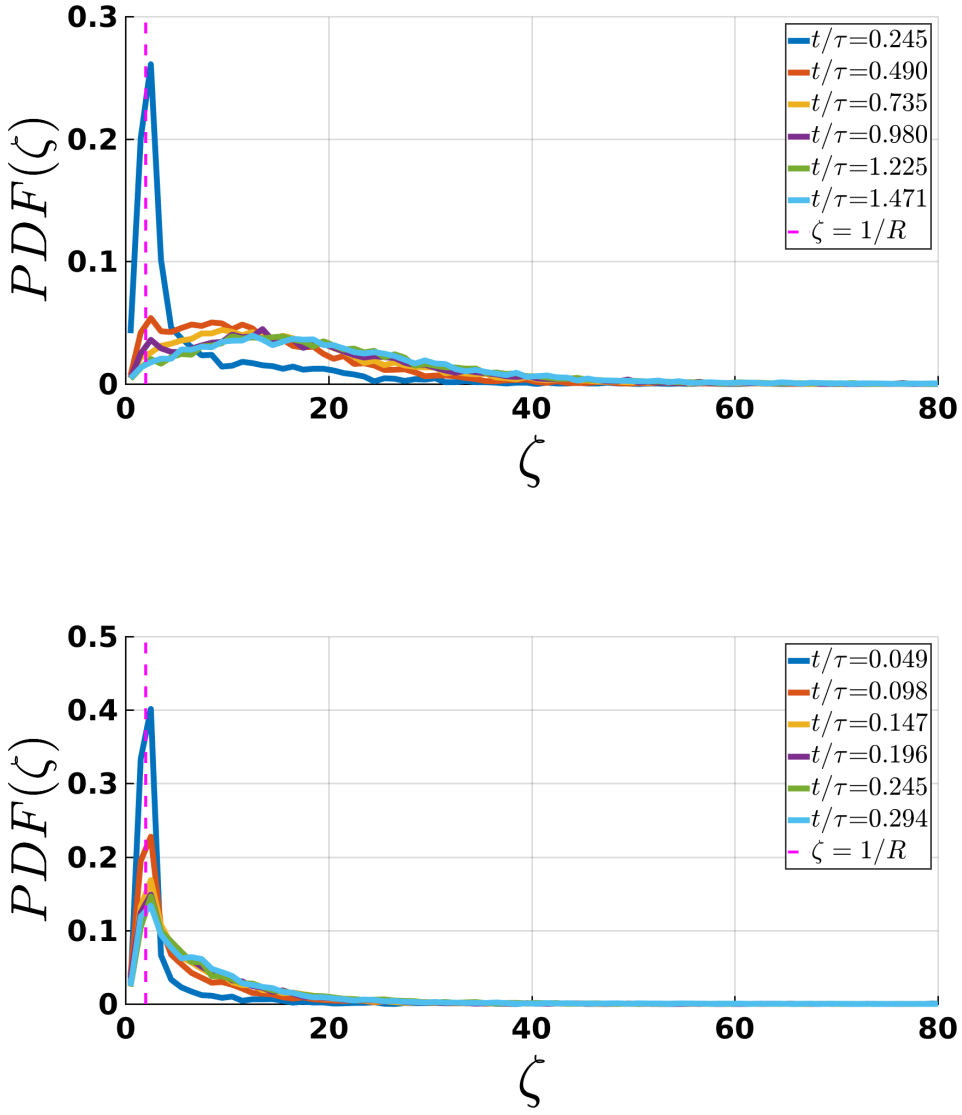


FIG. 7. Temporal evolution of the PDF of the curvature ζ (in cm^{-1}) for $Re_s = 29$ and $\dot{L}_{inj} = 3.35\text{cm}^{-2}\text{s}^{-1}$ (top) and $Re_s = 1.25$ and $\dot{L}_{inj} = 22.50\text{cm}^{-2}\text{s}^{-1}$ (bottom). In both simulations, at saturation the vortex line density $\overline{L}$ is approximately equal to 120cm^{-2} and the radius of the injected vortex rings is $R = D/2$. We clearly observe the generation of smaller scale structures when Re_s is larger.

Appendix E: Alternative normalisation for Vinen turbulence

In Fig. 3 (a), the energy dissipation rates of all data sets are normalised by the traditional factor $\langle I\rangle/\langle U\rangle^3$ used in classical turbulence. This is because the main result (the red curve) refers to a regime of quantum turbulence with the classical property that there is an inertial range where a dissipationless cascade takes place.

Fig. 3 (a) shows also data (green and blue curves) which refer to regimes of Vinen-like quantum turbulence: the same flattening of $\widetilde{\epsilon}$ at increasing Re_s is apparent because the analogy to the classical dissipation anomaly is independent of the dynamics at the large scales of the flow. It is however natural to ask how the curves would look using an alternative normalisation. A dedicated normalisation factor for Vinen turbulence would be the characteristic dissipation rate at scales comparable to the inter-vortex distance ℓ, given by $\epsilon_\ell = v_s(\ell)^3/\ell \sim \kappa^3\overline{L}^2$. Using this normalisation factor, the resulting dissipation rate still resembles the classical counterpart, as shown for example in Fig. 8.

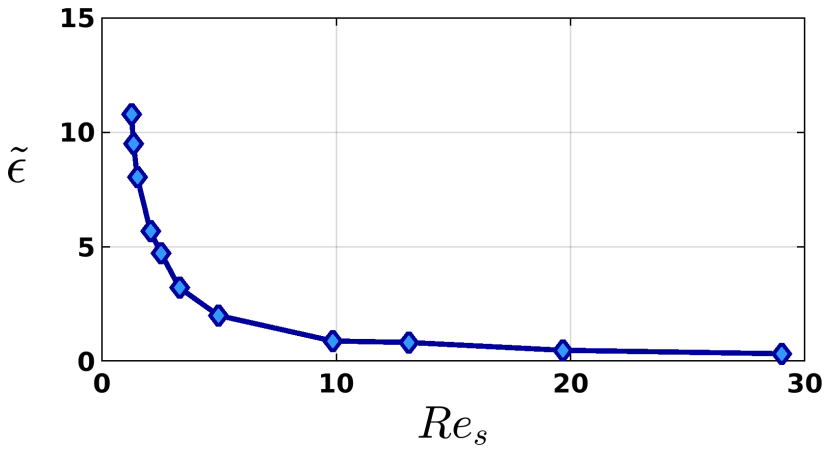


FIG. 8. Time-averaged energy dissipation ϵ for Vinen turbulence obtained by injecting vortex rings of radius $R = \ell/2$, corresponding to the blue curve of Fig 3(a), normalised by $\epsilon_\ell = v_s(\ell)^3/\ell \sim \kappa^3 \overline{L}^2$.

Appendix F: Numerical resolution of the small length scales

As increasing Re_s excites smaller length scales along the vortex lines it is natural to ask whether our numerical discretization correctly resolves these small length scales. To assess our numerical resolution we have repeated all the simulations replacing δ with $\delta/2$. In the analysis which leads to the calculation of $\widetilde{\epsilon}$ (Fig. 3(a)), we have rejected the results of the simulations, identified by the pair $(Re_s, \dot{L}_{inj})$, which do not satisfy either of the following strict criteria: (i) the saturation value $\overline{L}$ obtained using the two numerical resolutions are within 8% of each other, and (ii) the PDFs of the curvature ζ overlap. The first criterion ensures that the turbulent intensity is correctly captured, while the second is necessary in order to resolve accurately the curvature, which governs the dissipation (Eq. 7). For example, Fig. 9 (b) shows that for $(Re_s = 29, \dot{L}_{inj} = 3.35\text{cm}^{-2}\text{s}^{-1})$ the PDFs of the curvature do indeed overlap, hence criterion (ii) is satisfied, while this is not the case for $(Re_s = 49.45, \dot{L}_{inj} = 1.0\text{cm}^{-2}\text{s}^{-1})$, see Fig. 9 (a). In Fig. 9 (c) and (d) we report the correspondent temporal evolution of the vortex-line density, showing the impact of the resolution on this integral quantity: in terms of criterion (i) simulation $(Re_s = 49.45, \dot{L}_{inj} = 1.0\text{cm}^{-2}\text{s}^{-1})$ lacks of spatial resolution along the vortex-lines, while simulation $(Re_s = 29, \dot{L}_{inj} = 3.35\text{cm}^{-2}\text{s}^{-1})$ is sufficiently resolved.

We remark that this is the first time that such as strict criterion has been used to test the VFM at low temperatures or at high vortex line density; all previous work was mainly concerned with properties at the large length scales, whereas here we are primarily concerned with the smaller dissipation length scales. In practice, our strict criterion limits us to temperatures above $T \approx 1.3$ K, above [25, 27, 33] the appearance of scaling behaviour for the KW cascade [30–32], which, in the absence of dissipation, would shift energy to length scales of the order of a_0, not computationally resolvable by the VFM. At such short scales acoustic emission [42] and excitations of Carol-Matricon states dissipate the turbulent kinetic energy.

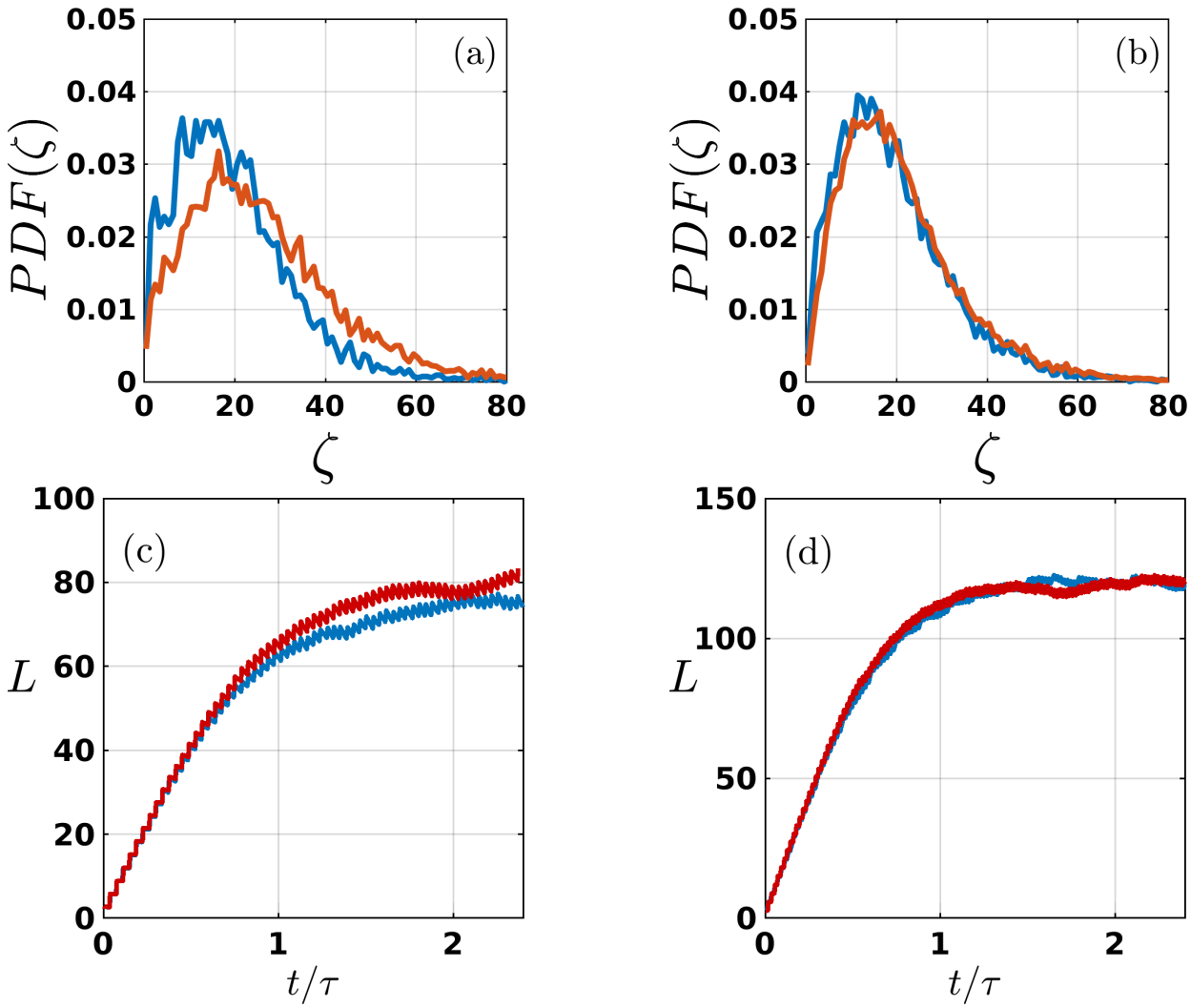


FIG. 9. Left (right) column refers to simulation where $Re_s = 49.45$ and $\dot{L}_{inj} = 1.0\text{cm}^{-2}\text{s}^{-1}$ ($Re_s = 29$ and $\dot{L}_{inj} = 3.35\text{cm}^{-2}\text{s}^{-1}$). Blue (red) curves refer to spatial discretization $\delta = 0.02$ cm ($\delta = 0.01$ cm). (a) and (b): PDF(ζ) (in cm) *vs* curvature ζ (in cm^{-1}); (c) and (d): vortex-line density L (in cm^{-2}) *vs* rescaled time t/τ, where $\tau = 2\pi/(\kappa\bar{L})$, $\bar{L}$ being the vortex-line density at saturation.

[1] K.R. Sreenivasan, On the scaling of the turbulence energy dissipation rate, Phys. Fluids **27**, 1048 (1984).
[2] Y. Kaneda, T. Ishihara, M. Yokokawa, K. Itakura and A. Uno, Energy dissipation rate and energy spectrum in high resolution direct numerical simulations of turbulence in a periodic box. Phys. Fluids **15** L21 (2003)
[3] L. Onsager, Statistical hydrodynamics, Nuovo Cimento, Suppl. **6**, 279 (1949).
[4] G.L. Eyink and K.R. Sreenivasan, Onsager and the theory of hydrodynamic turbulence, Rev. Modern Phys. **78**, 87 (2006).
[5] C.F. Barenghi, V. L'vov, and P.-E. Roche, Experimental, numerical and analytical velocity spectra in turbulent quantum fluid, Proc. Nat. Acad. Sci. USA, **111** (suppl. 1) 4683 (2014).
[6] S. R. Stakp, L. Skrbek and R. J. Donnelly, Decay of Grid Turbulence in a Finite Channel, Phys Rev Lett **82**, 4831 (1999)
[7] J. Maurer and P. Tabeling, Local investigation of superfluid turbulence, Europhys Lett **43**, 29 (1998).
[8] J. Salort, C. Baudet, B. Castaing, B. Chabaud, F. Daviaud, T. Didelot, P. Diribarne, B. Dubrulle, Y. Gagne, F. Gauthier, A. Girard, B Henbral, B. Rousset, P. Thibault, P.E. Roche, Phys Fluids **22**, 125102 (2020)
[9] A.N. Kolmogorov, The Local Structure of Turbulence in an Incompressible Viscous Fluid for Very Large Reynolds Numbers, Dokl. Akad. Nauk. SSSR **30**, 301 (1941)
[10] C.F. Barenghi, W.F. Vinen and R.J. Donnelly, Friction on quantized vortices in helium II: a review, J. Low Temp. Phys. **52**, 189 (1982).
[11] C. Nore, M. Abid and M.E. Brachet, Kolmogorov turbulence in low-temperature superflows, Phys. Rev. Lett. **78**, 3896

(1997).
[12] R.N. Hills & P.H. Roberts, Superfluid mechanics for a high density of vortex lines, Arch. Rat. Mech. Anal. **66**, 43 (1977).
[13] A.P. Finne, T.Araki, R. Blaauwgeers, V.B. Eltsov, N.B. Kopnin, M. Krusius, L. Skrbek, M. Tsubota & G.E. Volovik, An intrinsic velocity-independent criterion for superfluid turbulence, Nature **424**, 1022 (2003).
[14] K.W. Schwarz, Three-dimensional vortex dynamics in superfluid ^{4}He: homogeneous superfluid turbulence, Phys. Rev. B **38**, 2398 (1988).
[15] R. Hänninen and A.W. Baggaley, Vortex filament method as a tool for computational visualization of quantum turbulence, Proc. Nat. Acad. Sci. USA **111** (suppl. 1), 4667 (2014).
[16] K. W. Schwarz, Three-dimensional vortex dynamics in superfluid He 4: Line-line and line-boundary interactions Phys. Rev. B **31**, 5782 (1985).
[17] D. Kivotides, C.F. Barenghi, and D.C. Samuels, Triple vortex ring structure in superfluid helium II, Science **290** 777 (2000).
[18] L. Galantucci, A.W. Baggaley, C.F. Barenghi, and G. Krstulovic, A new self-consistent approach of quantum turbulence in superfluid helium Eur. Phys. J. Plus **135**, 1 (2020).
[19] L. Galantucci, G. Krstulovic, and C.F. Barenghi, Friction-enhanced lifetime of bundled quantum vortices, arXiv:2107.07768 (2022)
[20] D. Kivotides, Relaxation of superfluid vortex bundles via energy transfer to the normal fluid, Phys. Rev. B **76**, 054503 (2007).
[21] K. Morris, J, Koplik, and D.W.L. Rousen, Vortex locking in direct numerical simulations of quantum turbulence, Phys. Rev. Lett. **101**, 015301 (2008).
[22] P. M. Walmsley and A. I. Golov, Quantum and quasiclassical types of superfluid turbulence, Phys. Rev. Lett. **100**, 245301 (2008).
[23] A. Leonard, Computing three dimensional incompressible flows with votrex elements, Ann. Rev. Fluid Mech. **17**, 523 (1985).
[24] O. Yurkina and S. K. Nemirovskii, On the energy spectrum of the 3D velocity field, generated by an ensemble of vortex loops, Low Temp. Phys. **47**, 652 (2021).
[25] P. M. Walmsley, D.E. Zmeev, F. Pakpour, and A.I. Golov, Dynamics of quantum turbulence of different spectra, Proc Natl Acad Sci USA **111**, 4691 (2014)
[26] L. Skrbek and K.R. Sreenivasan, Developed quantum turbulence and its decay, Phys. Fluids **24**, 011301 (2012).
[27] W. F. Vinen, Theory of quantum grid turbulence in superfluid ^{3}He-B, Phys. Rev. B **71**, 024513 (2005).
[28] V. S. L'vov, S. V. Nazarenko and G. E. Volovik Energy Spectra of Developed Superfluid Turbulence JETP Letters **80**, 479 (2004)
[29] L. Skrbek, Phenomenology of quantum turbulence in superfluid helium, Proc. Natl. Acad. Sci. USA **116**, e2018406118 (2021).
[30] E.V. Kozik and B.V. Svistunov, Kelvin-wave cascade and decay of superfluid turbulence, Phys. Rev. Lett. **92**, 035301 (2004).
[31] V.S. L'vov and S.V. Nazarenko, Spectrum of Kelvin-wave turbulence in superfluids, JETP Lett. **91**, 428 (2010).
[32] G. Krstulovic, Kelvin-wave cascade and dissipation in low-temperature superfluid vortices Phys. Rev. E **86**, 055301(R) (2012).
[33] W. F. Vinen and J. J. Niemela, Quantum Turbulence, J Low Temp. Phys. **128**, 167 (2002).
[34] W. F. Vinen, Mutual Friction in a heat current in liquid helium II. III. Theory of mutual friction, Proc. R. Soc. London A **242**, 493 (1957).
[35] J. Gao, W. Guo, S. Yui, M. Tsubota, W. F. Vinen, Dissipation in quantum turbulence in superfluid ^{4}He above 1 K Phys. Rev. B **97**, 184518 (2018).
[36] C. F. Barenghi, R. J. Donnelly and W. F. Vinen, Friction on Quantized Vortices in Helium II. A Review J. Low Temp. Phys. **52**, 189 (1983).
[37] A. W. Baggaley, C. F. Barenghi, and Y. A. Sergeev, Quasiclassical and ultraquantum decay of superfluid turbulence, Phys. Rev. B **85**, 060501(R) (2012)
[38] T. Araki, M. Tsubota, and S.K. Nemirovskii, Energy spectrum of superfluid turbulence with no normal-fluid component, Phys. Rev. Lett. **89**, 145301 (2002).
[39] J.T. Makinen, S. Autti, P.J. Heikkinen, J.J. Hosio, R. Hänninen, V.S. L'vov, P.M. Walmsley, V.V. Zavjalov, and V.B. Eltsov Rotating quantum wave turbulence arXiv:2203.11527 (2022)
[40] J.P. John, D.A. Donzis, and K.R. Sreenivasan, Does dissipative anomaly hold for compressible turbulence?, J. Fluid Mech. **920**, A20 (2021)
[41] R.J. Donnelly and C.F. Barenghi, The observed properties of liquid helium at saturated vapour pressure, J. Phys. Chem. Ref. Data **27**, 1217 (1998)
[42] W. J. Kwon, G. Del Pace, K. Xhani, L. Galantucci, A. Muzi Falconi, M. Inguscio, F. Scazza and G. Roati Sound emission and annihilations in a programmable quantum vortex collider. Nature **600**, 64 (2021).